

# Coupled Dynamic Analysis and Equivalent Static Wind Loads on Buildings with Three-Dimensional Modes

Xinzhong Chen<sup>1</sup> and Ahsan Kareem<sup>2</sup>

**Abstract:** Buildings with either complex geometric shapes or structural systems with noncoincident centers of mass and resistance, or both, may undergo three-dimensional (3D) coupled motions when exposed to spatiotemporally varying dynamic wind loads. To capture the dynamic load effects, this paper presents a framework for the analysis of 3D coupled dynamic response of buildings and modeling of the equivalent static wind loads (ESWLs). This framework takes into account the correlation among wind loads in principle directions and the intermodal coupling of modal response components. The wind loading input for this scheme may be derived either from multiple point synchronous scanning of pressures on building models or through high-frequency force balance (HFFB) measurements. The ESWL for a given peak response is expressed as a linear combination of the background and resonant loads, which respectively reflect the fluctuating wind load characteristics and inertial loads in fundamental modes of vibration. The nuances of utilizing HFFB measurements for buildings with 3D coupled mode shapes are elucidated with a focus on the evaluation of the generalized forces including mode shape corrections, the background and resonant responses, and the associated ESWLs. Utilizing a representative tall building with 3D mode shapes and closely spaced frequencies, the framework for the analysis of coupled dynamic load effects and modeling of 3D ESWLs is demonstrated.

**DOI:** 10.1061/(ASCE)0733-9445(2005)131:7(1071)

**CE Database subject headings:** Wind loads; Wind tunnel tests; Building design; Structural dynamics; Random vibration; Dynamic analysis; Three-dimensional models.

## Introduction

Wind loads on buildings are manifested by the action of three-dimensional (3D) spatiotemporally varying random pressure fields on the building surface as the wind field interacts with the building. For wind speeds not in the proximity of the lock-in region for vortex-induced loads in the acrosswind direction and for loading scenarios that do not result in significant building motions, the aeroelastic effect can be neglected; therefore, wind loads can be regarded as an independent of building motion (e.g., ASCE 1999; Zhou and Kareem 2003). Accordingly, wind loads on buildings can be characterized through simultaneously measured pressures on the building model surfaces or by measured base forces on the model mounted on a high-frequency force balance (HFFB).

For buildings with one-dimensional (1D) mode shape in each primary direction, building response in each respective direction can be studied separately without the consideration of crosscorrelation of wind loads acting in different directions. However,

buildings with complex geometric shapes or with structural systems having noncoincident centers of mass and resistance, or both, may result in 3D coupled mode shapes and experience coupled responses when exposed to wind loads. Furthermore, frequencies in the fundamental modes of vibration in three primary directions may be closely spaced. These situations warrant a 3D coupled response analysis framework for response predictions that take into account the crosscorrelation of wind loads acting in different directions and the intermodal coupling of modal responses (e.g., Kareem 1985; Tallin and Ellingwood 1985; Shimada et al. 1990; Flay et al. 1999).

The HFFB technique has widely been recognized for conveniently quantifying generalized forces on buildings with uncoupled mode shapes through measured base forces on stationary-scaled building models (e.g., Kareem and Cermak 1979; Tschanz and Davenport 1983; Reinhold and Kareem 1986; Boggs and Peterka 1989). The generalized forces are then utilized for estimating dynamic response of buildings with given structural characteristics. The application of this technique to buildings with 3D coupled mode shapes has been discussed in Irwin and Xie (1993), Yip and Flay (1995), and Holmes et al. (2003) for the estimation of resonant response.

Current design practice often requires dynamic wind loads on buildings to be modeled as equivalent static wind loads (ESWLs). Accordingly, a relatively simple static structural analysis procedure can be adopted for a more detailed structural analysis and design. The ESWL description is not only utilized for modeling wind loads in building codes and standards, but also serves as a useful tool of better describing wind tunnel data derived for design applications. The gust response factor (GRF) approach, introduced by Davenport (1967) for alongwind excited buildings, has been used worldwide in building codes and standards. Similarly, GRFs can be defined for acrosswind and torsional response

<sup>1</sup>Assistant Professor, Wind Science and Engineering Research Center, Dept. of Civil Engineering, Texas Tech Univ., Lubbock, TX 79409. E-mail: xinzhong.chen@ttu.edu

<sup>2</sup>Robert M. Moran Professor, Dept. of Civil Engineering and Geological Sciences, Univ. of Notre Dame, Notre Dame, IN 46556. E-mail: kareem@nd.edu

Note. Associate Editor: Kurtis R. Gurley. Discussion open until December 1, 2005. Separate discussions must be submitted for individual papers. To extend the closing date by one month, a written request must be filed with the ASCE Managing Editor. The manuscript for this paper was submitted for review and possible publication on November 11, 2003; approved on September 24, 2004. This paper is part of the *Journal of Structural Engineering*, Vol. 131, No. 7, July 1, 2005. ©ASCE, ISSN 0733-9445/2005/7-1071-1082/\$25.00.

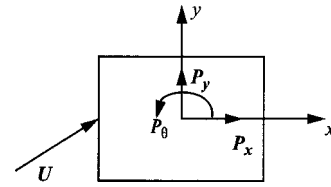


Fig. 1. Coordinate system and wind orientation

components with respect to a representative mean response, such as the alongwind mean response, while that leads to less physical meaning as compared to the GRF for the alongwind response (Piccardo and Solari 2000; Kareem and Zhou 2003). The GRF for a given response is defined as the ratio of its peak dynamic value to its mean (static) value. The GRF approach results in an ESWL that has a distribution similar to the mean wind load. As the actual ESWLs for different peak response components generally have different spatial distributions, the GRF depends on the response considered and may vary over a wide range for different response components (e.g., Holmes 1994; Chen and Kareem 2001, 2004; Zhou and Kareem 2001; Repetto and Solari 2004).

In order to cast a more convenient and physically meaningful ESWL description, dynamic wind loading is separated into background (quasi-static) and resonant components based on their frequency content (e.g., Davenport 1995). Based on this format, a number of studies have presented ESWLs on buildings with uncoupled responses. First, for the background ESWL (BESWL), Kasperski (1992) proposed a load-response-correlation (LRC) approach that results in a most probable load distribution while its spatial distribution varies for the response under consideration. An ESWL distribution identical for all response components, expressed in terms of a polynomial expansion, was suggested in Repetto and Solari (2004). Chen and Kareem (2004) proposed a gust loading envelope (GLE) approach, which provides a BESWL distribution similar to the GLE. For cases in which the distributions of the dynamic wind loads are unknown, but the integrated base forces are available using the HFFB technique, the BESWL can be approximately modeled by distributing the base bending moment over the building height. This is achieved by a distribution similar to the mean wind load (Boggs and Peterka 1989; Zhou and Kareem 2001) or similar to the modal inertial load (e.g., Xie et al. 1999). On the other hand, the resonant ESWL (RESWL) can be described in terms of modal inertial load in a straightforward and physically meaningful manner (e.g., Davenport 1985). A similar format has been utilized for modeling dynamic earthquake loads on buildings in codes and standards (e.g., ASCE 2002). The ESWL for the total peak response can be expressed as a linear combination of the background and resonant loads, which also offers convenient combination of wind load with other loads for design considerations (Boggs and Peterka 1989; Chen and Kareem 2001, 2004; Holmes 2002).

In this paper, a framework for the analysis of 3D coupled dynamic response and evaluation of associated ESWLs on buildings are presented on the basis of wind loads derived through either synchronous scanning of pressures on building surfaces or the HFFB measurements. The proposed framework takes into account the correlation among wind loads in principle directions and the intermodal coupling of modal response components. The application of HFFB technique to buildings with 3D coupled modes is revisited by focusing on the evaluation of the generalized forces with mode shape corrections, the background and resonant response, and associated ESWLs. A tall building with 3D mode shapes and closely spaced frequencies is used as an example to discuss the coupled dynamic response and to demonstrate the proposed framework.

### Analysis of Coupled Response and Modeling of Equivalent Static Wind Loads

In the following section, the analysis of the 3D coupled building dynamic response and the modeling of ESWL associated with any

peak response of interest are presented. The wind loads can be derived from a multiple point synchronously scanned pressure field over a building model surface in a wind tunnel.

### Mean and Background Responses

A building with 3D coupled mode shapes at a given wind speed and direction is considered (Fig. 1). The wind loads per unit height at the elevation  $z$  above the ground have mean components of  $\bar{P}_x(z)$ ,  $\bar{P}_y(z)$ , and  $\bar{P}_\theta(z)$ , and corresponding fluctuating components of  $P_x(z, t)$ ,  $P_y(z, t)$ , and  $P_\theta(z, t)$ , along two orthogonal translational primary axes,  $x$  and  $y$ , and about the vertical axis,  $z$ . Consider a specific response of interest at a building elevation  $z_0$ ,  $R(t)$ , e.g., displacement, bending moment, shear force, or other member forces. Its mean (static) and background (quasi-static) components can be calculated by static and quasi-static analyses, and are expressed as

$$\bar{R} = \int_0^H [\mu_x(z)\bar{P}_x(z) + \mu_y(z)\bar{P}_y(z) + \mu_\theta(z)\bar{P}_\theta(z)]dz \quad (1)$$

$$R_b(t) = \int_0^H [\mu_x(z)P_x(z, t) + \mu_y(z)P_y(z, t) + \mu_\theta(z)P_\theta(z, t)]dz \quad (2)$$

where  $\mu_s(z)$  ( $s=x, y, \theta$ )=influence function representing the response  $R$  due to a unit load acting at the elevation  $z$  along  $s$  direction; and  $H$ =building height.

The root-mean-square (RMS) background response is given by

$$\sigma_{R_b}^2 = \sum_{s=x, y, \theta} \sum_{l=x, y, \theta} \int_0^H \int_0^H \mu_s(z_1)\mu_l(z_2)R_{P_{sl}}(z_1, z_2)dz_1dz_2 \quad (3)$$

where  $R_{P_{sl}}(z_1, z_2)$ =covariance between  $P_s(z_1, t)$  and  $P_l(z_2, t)$ , and is related to their cross power spectra density (XPSD) function  $S_{P_{sl}}(z_1, z_2, f)$  by

$$R_{P_{sl}}(z_1, z_2) = \int_0^{f'} S_{P_{sl}}(z_1, z_2, f)df \approx \int_0^\infty S_{P_{sl}}(z_1, z_2, f)df \quad (4)$$

where  $f' \leq f_1$ , and  $f_1$ =first modal frequency of the building.

### Resonant Response

The resonant response is calculated through the modal analysis by retaining only the three fundamental modes in the primary directions with the assumption that the contribution from higher modes is negligible. The  $j$ th generalized force is expressed as

$$Q_j(t) = \int_0^H [\Theta_{jx}(z)P_x(z, t) + \Theta_{jy}(z)P_y(z, t) + \Theta_{j\theta}(z)P_\theta(z, t)]dz \quad (5)$$

where  $\Theta_{js}(z)$  ( $s=x, y, \theta$ )= $j$ th mode shape ( $j=1, 2, 3$ ).

The power spectral density (PSD) function of  $Q_j(t)$ ,  $S_{Q_{jj}}(f)$ , and the XPSD between  $Q_j(t)$  and  $Q_k(t)$ ,  $S_{Q_{jk}}(f)$ , are expressed as

$$S_{Q_{jj}}(f) = \sum_{s=x,y,\theta} \sum_{l=x,y,\theta} \int_0^H \int_0^H \Theta_{js}(z_1) \Theta_{jl}(z_2) S_{P_{sl}}(z_1, z_2, f) dz_1 dz_2 \quad (6)$$

$$S_{Q_{jk}}(f) = \sum_{s=x,y,\theta} \sum_{l=x,y,\theta} \int_0^H \int_0^H \Theta_{js}(z_1) \Theta_{kl}(z_2) S_{P_{sl}}(z_1, z_2, f) dz_1 dz_2 \quad (7)$$

The RMS resonant component of the  $j$ th generalized displacement,  $\sigma_{q_{jr}}$ , is quantified as

$$\sigma_{q_{jr}}^2 = \int_{f'}^{\infty} |H_j(f)|^2 S_{Q_{jj}}(f) df \approx \frac{1}{M_j^2 (2\pi f_j)^4} \frac{\pi}{4\xi_j} f_j S_{Q_{jj}}(f_j) \quad (8)$$

$$H_j(f) = \frac{1}{M_j (2\pi f_j)^2 [1 - (f/f_j)^2 + 2i\xi_j f/f_j]} \quad (9)$$

$$M_j = \int_0^H [m(z) \Theta_{jx}^2(z) + m(z) \Theta_{jy}^2(z) + I(z) \Theta_{j\theta}^2(z)] dz \quad (10)$$

where  $M_j$ ,  $f_j$ , and  $\xi_j$ = $j$ th generalized mass, frequency, and damping ratio (including aerodynamic damping); and  $m(z)$  and  $I(z)$ =mass and polar moment of inertia per unit height.

The covariance between the  $j$ th and  $k$ th resonant modal responses,  $\sigma_{q_{jkr}}^2 = \sigma_{q_{kjr}}^2$  is given by

$$\sigma_{q_{jkr}}^2 = \text{Re} \left[ \int_{f'}^{\infty} H_j(f) H_k^*(f) S_{Q_{jk}}(f) df \right] = r_{jkr} \sigma_{q_{jr}} \sigma_{q_{kr}} \quad (11)$$

where Re and \* represent the real and complex conjugate operators, respectively;  $r_{jkr}$ =the correlation coefficient for the  $j$ th and  $k$ th resonant modal responses, which can be approximated by the following expression when  $f_j$  and  $f_k$  are close to each other:

$$r_{jkr} = \alpha_{jkr} \rho_{jkr} \quad (12)$$

$$\alpha_{jkr} = \text{Re} \left[ (S_{Q_{jk}}(f)) / \sqrt{S_{Q_{jj}}(f) S_{Q_{kk}}(f)} \right]_{f=f_j \text{ or } f_k} \quad (13)$$

and  $\rho_{jkr}$  is given in Der Kiureghian (1980)

$$\rho_{jkr} = \frac{8\sqrt{\xi_j \xi_k} (\beta_{jk} \xi_j + \xi_k) \beta_{jk}^{3/2}}{(1 - \beta_{jk}^2)^2 + 4\xi_j \xi_k \beta_{jk} (1 + \beta_{jk}^2) + 4(\xi_j^2 + \xi_k^2) \beta_{jk}^2} \quad (14)$$

where  $\beta_{jk} = f_j/f_k$  with  $\rho_{jkr}$  ( $0 \leq \rho_{jkr} \leq 1$ ),  $\rho_{jkr} = \rho_{kkr} = 1$  and  $\rho_{jkr} = \rho_{kjr} \ll 1$  when  $f_j$  and  $f_k$  are well separated. It should be noted that in the case of seismic response of buildings with a single ground motion input,  $\alpha_{jkr}$  is either +1 or -1 for  $j \neq k$  depending upon the sign of  $\text{Re}[S_{Q_{jk}}(f)]$  at  $f_j$  or  $f_k$ . In general,  $-1 \leq \alpha_{jkr} \leq 1$ . It is clear that the correlation coefficient of modal responses depends not only on the modal frequencies and damping ratios, but also on the correlation/coherence of the associated generalized forces. This important consideration for accurate utilization of the complete quadratic combination (CQC) scheme has not been completely recognized in the analysis of wind load effects on buildings and structures (e.g., Xie et al. 2003).

Once the generalized displacement is quantified, the resonant response of interest,  $R_r(t)$ , is given by

$$R_r(t) = \sum_{j=1}^3 R_{jr}(t) = \sum_{j=1}^3 \Gamma_j q_{jr}(t) \quad (15)$$

$$\Gamma_j = (2\pi f_j)^2 \int_0^H [\mu_x(z) m(z) \Theta_{jx}(z) + \mu_y(z) m(z) \Theta_{jy}(z) + \mu_\theta(z) I(z) \Theta_{j\theta}(z)] dz \quad (16)$$

where  $R_{jr}(t) = \Gamma_j q_{jr}(t)$ =contribution of the  $j$ th mode to  $R_r(t)$ ;  $\Gamma_j$ =participation coefficient of the  $j$ th mode to  $R_r(t)$ , which represents the static response to the  $j$ th modal inertial load associated with a unit generalized displacement ( $\sigma_{q_{jr}} = 1$ ).

The RMS resonant response,  $\sigma_{R_r}$ , is given by combining the modal components using the CQC approach:

$$\sigma_{R_r}^2 = \sum_{j=1}^3 \sum_{k=1}^3 \sigma_{R_{jr}} \sigma_{R_{kr}} r_{jkr} = \sum_{j=1}^3 \sum_{k=1}^3 \Gamma_j \Gamma_k \sigma_{q_{jr}} \sigma_{q_{kr}} r_{jkr} \quad (17)$$

When the modal frequencies are well separated, the intermodal coupling among modal response components can be neglected, i.e.,  $r_{jkr} = 1$  for  $j=k$  and  $r_{jkr} = 0$  for  $j \neq k$ . Consequently, in that case, the modal responses can be combined using the square root of the sum of squares (SRSS) combination scheme.

### Total Peak Response

The peak dynamic response,  $R_{\max}$ , can be obtained by combining the background and resonant components:

$$R_{\max} = \sqrt{g_b^2 \sigma_{R_b}^2 + g_r^2 \sigma_{R_r}^2} \quad (18)$$

where  $g_b$  and  $g_r$ =peak factors for the background and resonant responses, generally ranging from 3 to 4.

The total peak response including the mean component is equal to  $\bar{R} \pm R_{\max}$ .

### Background Equivalent Static Wind Load

Based on the LRC approach (Kasperski 1992; Holmes 2002), a 3D BESWL for the peak background response,  $R_{b \max} = g_b \sigma_{R_b}$ , can be expressed as

$$F_{eR_{bs}}(z) = \frac{g_b}{\sigma_{R_b}} \sum_{l=x,y,\theta} \int_0^H \mu_l(z_1) R_{P_{sl}}(z, z_1) dz_1 \quad (s = x, y, \theta) \quad (19)$$

where  $F_{eR_{bs}}(z)$ =BESWL component along  $s$  direction ( $s = x, y, \theta$ ).

The LRC approach results in a most probable load distribution for a given peak background response. However, a different load distribution corresponds to each response component, which may limit its potential attractiveness for possible adoption by design standards or practice. An approximate modeling of the BESWL based on the LRC approach for uncoupled buildings has been presented in Holmes (1996) by eliminating the effect of the influence function of the response.

Chen and Kareem (2004) proposed the GLE approach for modeling BESWL for 3D excited buildings with uncoupled response which eliminates the potential shortcoming of the LRC approach. This approach can be extended to general coupled cases. The background response given in Eq. (3) can be represented by

$$\sigma_{R_b}^2 = \sum_{s=x,y,\theta} \sum_{l=x,y,\theta} \sigma'_{R_{bs}} \sigma'_{R_{bl}} B_{sl} \quad (20)$$

$$B_{sl} = \int_0^H \int_0^H \mu_s(z_1) \mu_l(z_2) R_{P_{sl}}(z_1, z_2) dz_1 dz_2 / (\sigma'_{R_{b^s}} \sigma'_{R_{b^l}}) \quad (21)$$

$$\sigma'_{R_{b^s}} = \int_0^H \mu_s(z) \sigma_{P_s}(z) dz \quad (22)$$

where  $\sigma'_{R_{b^s}}$  = response  $R$  to the static load  $\sigma_{P_s}(z)$ ;  $\sigma_{P_s}(z) = \sqrt{R_{P_{ss}}(z, z)}$  = the RMS value of wind load  $P_s(z)$ ; and  $B_{sl}$  = background factor representing the reduction effect with regard to response  $R$  due to loss of correlation in wind loads acting in  $s$  and  $l$  directions, which becomes unity when wind loads are fully correlated, i.e.,  $R_{P_{sl}}(z_1, z_2) = \sigma_{P_s}(z_1) \sigma_{P_l}(z_2)$ .

Eq. (20) can be rewritten as

$$g_b \sigma_{R_b} = \sum_{s=x,y,\theta} \int_0^H \mu_s(z) F'_{eR_{b^s}}(z) dz \quad (23)$$

that leads to BESWL given by

$$F'_{eR_{b^s}}(z) = F'_{ebs}(z) W_{R_{b^s}} \quad (24)$$

$$F'_{ebs}(z) = g_b \sigma_{P_s}(z) \quad (25)$$

$$W_{R_{b^s}} = \left( \sum_{l=x,y,\theta} B_{sl} \sigma'_{R_{bl}} \right) / \sigma_{R_b} \quad (26)$$

where  $F'_{ebs}(z)$  = gust loading envelope in  $s$  direction ( $s=x, y, \theta$ ).

It is worth emphasizing that the GLE approach results in a load distribution similar to the gust loading envelope for each response component. When wind loads are fully correlated, then  $B_{sl} = 1$  and  $W_{R_{b^s}} = 1$ , which leads to the load distribution identical to the gust loading envelope and to that given by the LRC approach.

### Resonant Equivalent Static Wind Load

The RESWL for the peak resonant response in the  $j$ th mode,  $R_{j\max} = g_r \sigma_{R_{jr}} = g_r \Gamma_j \sigma_{q_{jr}}$ , is given in terms of the modal inertial load:

$$F_{ejrs}(z) = g_r (2\pi f_j)^2 m_s(z) \Theta_{js}(z) \sigma_{q_{jr}} \quad (s=x, y, \theta) \quad (27)$$

where  $m_x(z) = m_y(z) = m(z)$  and  $m_\theta(z) = I(z)$ .

The validity of the modal inertial loads can be simply reaffirmed by substituting these force components in the following equation

$$g_r \sigma_{R_{jr}} = \int_0^H [\mu_x(z) F_{ejrx}(z) + \mu_y(z) F_{ejry}(z) + \mu_\theta(z) F_{ejr\theta}(z)] dz \quad (28)$$

The RESWL can also be expressed in a format that distributes the base bending moments and torque over the building height as

$$F_{ejrs}(z) = \frac{m(z) \Theta_{js}(z)}{\int_0^H m(z) \Theta_{js}(z) dz} g_r \sigma_{M'_{jrs}} \quad (s=x, y) \quad (29)$$

$$F_{ejr\theta}(z) = \frac{I(z) \Theta_{j\theta}(z)}{\int_0^H I(z) \Theta_{j\theta}(z) dz} g_r \sigma_{M'_{jr\theta}} \quad (30)$$

where  $\sigma_{M'_{jrs}} = \Gamma_j M_s \sigma_{q_{jr}}$  = RMS value of  $j$ th modal component of resonant base bending moment or torque  $M'_{rs}(t)$  ( $s=x, y, \theta$ ).

### Total Equivalent Static Wind Load

The ESWL for the total peak response  $R_{\max}$  can be obtained by a linear combination of the BESWL and RESWL (Boggs and Peterka 1989; Chen and Kareem 2001, 2004; Holmes 2002). Using the BESWL based on the LRC approach, the ESWL is given as

$$F_{eRs}(z) = W_{R_b} F_{eR_{b^s}}(z) + \sum_{j=1}^3 W_{jR_r} F_{ejrs}(z) \quad (s=x, y, \theta) \quad (31)$$

Using the BESWL based on the GLE approach, the ESWL is given as

$$F_{eRs}(z) = W'_{R_{b^s}} F'_{ebs}(z) + \sum_{j=1}^3 W_{jR_r} F_{ejrs}(z) \quad (s=x, y, \theta) \quad (32)$$

where the weighting factors are defined as

$$W_{R_b} = g_b \sigma_{R_b} / R_{\max}; \quad W'_{R_{b^s}} = g_b \left( \sum_{l=x,y,\theta} \sigma'_{R_{bl}} B_{sl} \right) / R_{\max} \quad (33)$$

$$W_{jR_r} = g_r \left( \sum_{k=1}^3 \sigma_{R_{kr}} r_{jkr} \right) / R_{\max} \quad (34)$$

The validity of the preceding ESWL can be easily reaffirmed by

$$R_{\max} = \int_0^H (\mu_x(z) F_{eRx}(z) + \mu_y(z) F_{eRy}(z) + \mu_\theta(z) F_{eR\theta}(z)) dz \quad (35)$$

The total loading, including the mean load component, is equal to  $\bar{P}_s(z) \pm F_{eRs}(z)$  ( $s=x, y, \theta$ ).

### High-Frequency Force Balance Technique for Buildings with Three-Dimensional Coupled Modes

The HFFB technique has been very effective in quantifying generalized forces on tall buildings and structures with uncoupled modes. The following section sheds light on the utilization of HFFB technique for buildings with 3D coupled modes by focusing on the estimation of generalized forces with mode shape corrections, analysis of coupled response, and modeling of ESWL.

#### Generalized Forces

The HFFB technique is predicated on the estimation of the generalized forces obtained from the measured base forces. The base bending moments along axes  $x$  and  $y$  and torque around  $z$ ,  $M_s(t)$  ( $s=x, y, \theta$ ), can be expressed in terms of the dynamic wind loads as

$$M_s(t) = \int_0^H \mu_{M_s}(z) P_s(z, t) dz \quad (36)$$

where  $\mu_{M_x}(z) = \mu_{M_y}(z) = z$  = influence functions for  $M_x(t)$  and  $M_y(t)$ , respectively; and  $\mu_{M_\theta}(z) = 1$  = influence function for  $M_\theta(t)$ .

On the other hand, the  $j$ th generalized force is given by

$$Q_j(t) = Q_{jx}(t) + Q_{jy}(t) + Q_{j\theta}(t) \quad (37)$$

$$Q_{js}(t) = \int_0^H \Theta_{js}(z) P_s(z, t) dz \quad (s = x, y, \theta) \quad (38)$$

It is obvious that when the building mode shape along the translational directions,  $\Theta_{jx}(z)$  and  $\Theta_{jy}(z)$ , vary linearly, the component in torsion,  $\Theta_{j\theta}(z)$ , varies uniformly over the building height, i.e.

$$\Theta_{js}(z) = \Theta_{js0} \left( \frac{z}{H} \right) \quad (s = x, y); \quad \Theta_{j\theta}(z) = \Theta_{j\theta 0} \quad (39)$$

where  $\Theta_{js0}$  ( $s = x, y, \theta$ ) = constants;  $Q_{js}(t)$  is then directly determined from the base forces as

$$Q_{js}(t) = \frac{\Theta_{js0}}{H} M_s(t) \quad (s = x, y); \quad Q_{j\theta}(t) = \Theta_{j\theta 0} M_\theta(t) \quad (40)$$

or in terms of their power spectral density (PSDs) as

$$S_{Q_{js}}(f) = \frac{\Theta_{js0}^2}{H^2} S_{M_s}(f) \quad (s = x, y); \quad S_{Q_{j\theta}}(f) = \Theta_{j\theta 0}^2 S_{M_\theta}(f) \quad (41)$$

While some buildings may have mode shapes in the translational directions that vary almost linearly over the building height, the component in torsion generally differs distinctly from a uniform variation over building height. For a general 3D mode shape with nonlinear variations in the translational directions and nonuniform in torsion, the relationship between  $Q_{js}(t)$  and  $M_s(t)$  can be defined by using their PSDs as

$$S_{Q_{js}}(f) = \eta_{js}^2(f) S_{M_s}(f) \quad (s = x, y, \theta) \quad (42)$$

where  $\eta_{js}(f)$  represents the mode shape correction that also depends on the manner in which the mode shape is normalized. It is expressed in terms of the dynamic wind loads as

$$\eta_{js}^2(f) = \frac{\int_0^H \int_0^H \Theta_{js}(z_1) \Theta_{js}(z_2) S_{P_{ss}}(z_1, z_2, f) dz_1 dz_2}{\int_0^H \int_0^H \mu_{M_s}(z_1) \mu_{M_s}(z_2) S_{P_{ss}}(z_1, z_2, f) dz_1 dz_2} \quad (43)$$

The XPSD between wind loads acting at different locations but in the same direction are often assumed to be real-valued. This results in a real-valued XPSD between  $Q_{js}(t)$  and  $M_s(t)$  and real-valued  $\eta_{js}(f)$  ( $s = x, y, \theta$ ). Consequently, the XPSD between  $Q_{js}(t)$  and  $Q_{kl}(t)$  ( $j, k = 1, 2, 3$ ;  $s, l = x, y, \theta$ ),  $S_{Q_{jksl}}(f)$ , can be expressed in terms of the XPSD between the respective base moments  $M_s(t)$  and  $M_l(t)$ ,  $S_{M_{sl}}(f)$ , as

$$S_{Q_{jksl}}(f) = \eta_{js}(f) \eta_{kl}(f) S_{M_{sl}}(f) \quad (44)$$

Accordingly, the PSD of  $Q_j(t)$  and the XPSD between  $Q_j(t)$  and  $Q_k(t)$  are given by

$$S_{Q_{jj}}(f) = \sum_{s=x,y,\theta} \sum_{l=x,y,\theta} \eta_{js}(f) \eta_{jl}(f) S_{M_{sl}}(f) \quad (45)$$

$$S_{Q_{jk}}(f) = \sum_{s=x,y,\theta} \sum_{l=x,y,\theta} \eta_{js}(f) \eta_{kl}(f) S_{M_{sl}}(f) \quad (46)$$

It is noted that the XPSD of wind loads acting in different directions does not influence the mode shape corrections. The mode shape corrections used in the case of 1D uncoupled modes are applicable to 3D coupled modes. The quantification of mode shape corrections has to rely on empirical correction or analytical formulations derived based on a presumed analytical wind loading model (Vickery et al. 1985; Boggs and Peterka 1989; Xu and Kwok 1993; Zhou et al. 2002; Holmes et al. 2003; Chen and Kareem 2004). For example, the XPSD of wind loads acting in the  $s$  direction  $P_s(z_1, t)$  and  $P_s(z_2, t)$ ,  $S_{P_{ss}}(z_1, z_2, f)$ , and the component of the  $j$ th mode shape in the  $s$  direction are described by

$$S_{P_{ss}}(z_1, z_2, f) = \frac{S_{P_{s0}}(f)}{H^2} \left( \frac{z_1}{H} \right)^{\alpha_s} \left( \frac{z_2}{H} \right)^{\alpha_s} \exp\left( -\frac{k_{zs} f |z_1 - z_2|}{U_H} \right) \quad (47)$$

$$\Theta_{js}(z) = \Theta_{js0} \left( \frac{z}{H} \right)^{\beta_s} \quad (48)$$

Accordingly, the mode shape correction can be given by the following closed-form expression (Chen and Kareem 2003)

$$\eta_{js} = \left( \frac{\Theta_{js0}}{H^{\beta_s}} \right) \left( \frac{1 + \alpha_s + \beta_s'}{1 + \alpha_s + \beta_s} \right) \sqrt{\frac{1 + k_{zs} f H / U_H / (2.5 + \beta_s')}{1 + k_{zs} f H / U_H / (2.5 + \beta_s)}} \quad (49)$$

where  $S_{P_{s0}}(f)$  = PSD of wind loads at the building height;  $k_{zs}$  = decay factor;  $U_H$  = mean wind speed at the building top;  $\alpha_s$  = exponent of wind load profile;  $\beta_s$  = mode shape exponent;  $\beta_s' = 1$  when  $s = x$  or  $y$ ; and  $\beta_s' = 0$  when  $s = \theta$ . It can be shown that when  $k_{zs} f H / U_H \rightarrow 0$ , which corresponds to full coherence of wind loads, the mode shape correction is the same as suggested in Xu and Kwok (1993) and discussed in Holmes et al. (2003).

It should be noted that when the actual building mode shape is known and if it departs distinctly from a power law, fitting the mode shape in terms of a power law, in order to use the closed-form formulation of mode shape correction, may result in additional approximation. Therefore, it is suggested to directly quantify the mode shape correction through a numerical calculation based on its definition given by Eq. (43) and using an assumed loading model.

It is worth mentioning that when the frequency dependent mode shape corrections are simplified as independent of frequency, the equivalent time domain version of Eqs. (45) and (46) can be expressed by (e.g., Irwin and Xie 1993; Holmes et al. 2003)

$$Q_j(t) = \eta_{jx} M_x(t) + \eta_{jy} M_y(t) + \eta_{j\theta} M_\theta(t) \quad (50)$$

### Dynamic Response and Equivalent Static Wind Load

The HFFB provides direct measurements of the background base bending moments and torque. However, other background response components need to be evaluated. While the background response is more likely to be contributed by higher modes as compared to the resonant response, it is still reasonable for tall buildings to assume that the contributions of higher modes to both the background and resonant responses are rather small. There-

fore, both the background and resonant response components can be approximately estimated by the modal analysis restricted to the fundamental modes.

The background component of the  $j$ th generalized displacement,  $\sigma_{q_{jb}}$ , and the correlation coefficient for the  $j$ th and  $k$ th background modal responses,  $r_{jkb}$ , are given by

$$\sigma_{q_{jb}} = \frac{\sigma_{Q_{jj}}}{M_j(2\pi f_j)^2} \quad (51)$$

$$r_{jkb} = \sigma_{q_{jkb}}^2 / \sqrt{\sigma_{q_{jb}} \sigma_{q_{kb}}} = \sigma_{Q_{jk}}^2 / \sqrt{\sigma_{Q_{jj}} \sigma_{Q_{kk}}} \quad (52)$$

$$\sigma_{Q_{jk}}^2 = \int_0^\infty \text{Re}[S_{Q_{jk}}(f)] df \quad (j, k = 1, 2, 3) \quad (53)$$

where  $\sigma_{Q_{jj}}^2$  and  $\sigma_{Q_{jk}}^2$  = variance of  $Q_j(t)$  and the covariance between  $Q_j(t)$  and  $Q_k(t)$ , respectively.

The background response can also be directly quantified from measured base bending moments and torque without introducing any correction procedure. Based on the modal analysis, the covariance of base bending moments and base torque,  $\sigma_{M_{sl}}^2$  ( $s, l = x, y, \theta$ ), can be expressed in terms of the covariance of the background modal response,  $\sigma_{q_{jkb}}^2$  ( $j, k = 1, 2, 3$ ), where  $\sigma_{q_{jlb}}^2 = \sigma_{q_{jb}}^2$  as

$$\sigma_{M_{sl}}^2 = \sum_{j=1}^3 \sum_{k=1}^3 \Gamma_{jM_s} \Gamma_{kM_l} \sigma_{q_{jkb}}^2 \quad (54)$$

$$\Gamma_{jM_s} = (2\pi f_j)^2 \int_0^H \mu_{M_s} m_s(z) \Theta_{js}(z) dz \quad (55)$$

Eq. (54) can be expressed in the matrix format, which leads to the solution of  $[\sigma_{q_{jkb}}^2]$  by

$$[\sigma_{q_{jkb}}^2] = [\Gamma_{jM_s}]^{-1} [\sigma_{M_{sl}}^2] [\Gamma_{jM_s}]^{-T} \quad (56)$$

The resonant modal response,  $\sigma_{q_{jkr}}^2$  ( $j, k = 1, 2, 3$ ), can be estimated using the framework discussed in preceding sections.

The total peak dynamic response of interest,  $R_{\max}$ , is obtained by combining the background and resonant response components:

$$R_{\max} = \sqrt{\sum_{j=1}^3 \sum_{k=1}^3 \Gamma_j \Gamma_k (g_b^2 \sigma_{q_{jkb}}^2 + g_r^2 \sigma_{q_{jkr}}^2)} \\ = \sqrt{g \sum_{j=1}^3 \sum_{k=1}^3 \Gamma_j \Gamma_k \sigma_{q_j} \sigma_{q_k} r_{jkb}} \quad (57)$$

$$\sigma_{q_j} = \sqrt{\sigma_{q_{jb}}^2 + \sigma_{q_{jkr}}^2} \quad (j = 1, 2, 3) \quad (58)$$

$$r_{jkb} = (g_b^2 r_{jkb} \sigma_{q_{jb}} \sigma_{q_{kb}} + g_r^2 r_{jkr} \sigma_{q_{jkr}} \sigma_{q_{kr}}) / (g \sigma_{q_j} \sigma_{q_k}) \quad (59)$$

The associated ESWL, including the background and resonant components, can be defined in terms of modal inertial loads, which may be represented by distributing the base bending moments and torque associated with each mode over the building height.

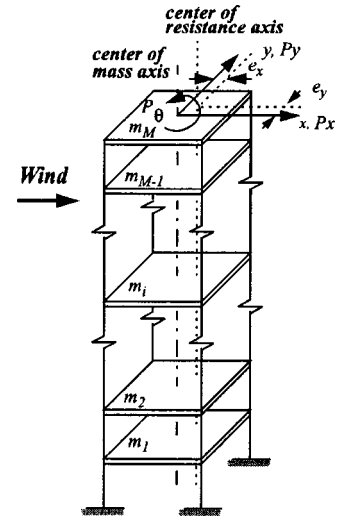


Fig. 2. Building with idealized eccentricity

## Application

### Three-Dimensional Coupled Response

A tall building with eccentricity in the centers of mass and resistance is taken as an example to discuss the coupled building motion and the associated ESWLs. The building is 31 m square in plan and 183 m tall with building density of 192 kg/m<sup>3</sup>. For the purpose of illustration, it is assumed that the mass centers of all floors lie on one vertical axis so that the eccentricity in the centers of mass and resistance at each story level is the same. All floors are assumed to have the same radius of gyration about the vertical axis through the mass center (Fig. 2). The equations of building motion are given in the Appendix (e.g., Kareem 1985).

The uncoupled building system (without eccentricity) has fundamental frequencies of 0.2 Hz in two translational directions, and 0.30 Hz in torsion. The corresponding mode shapes follow power functions along the building height, i.e.,  $\Psi_x(z) = \Psi_y(z) = \Psi_\theta(z) = (z/H)^{1.2}$ . The coupled building system has the eccentricity as  $e_x/r = e_y/r = -0.20$ , where  $e_x$  and  $e_y$  are the distance between the mass and resistance centers in two translational directions, and  $r = 31/2/\sqrt{6} = 6.3278$  m is the radius of gyration. The presence of eccentricity results in 3D coupled mode shapes of vibration. The three fundamental modal

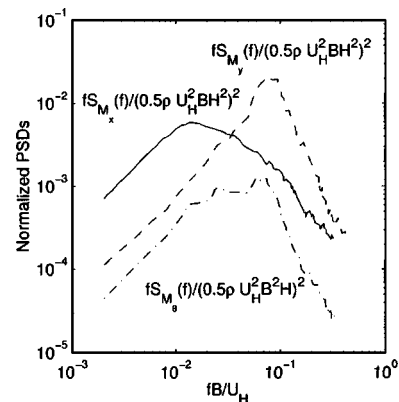
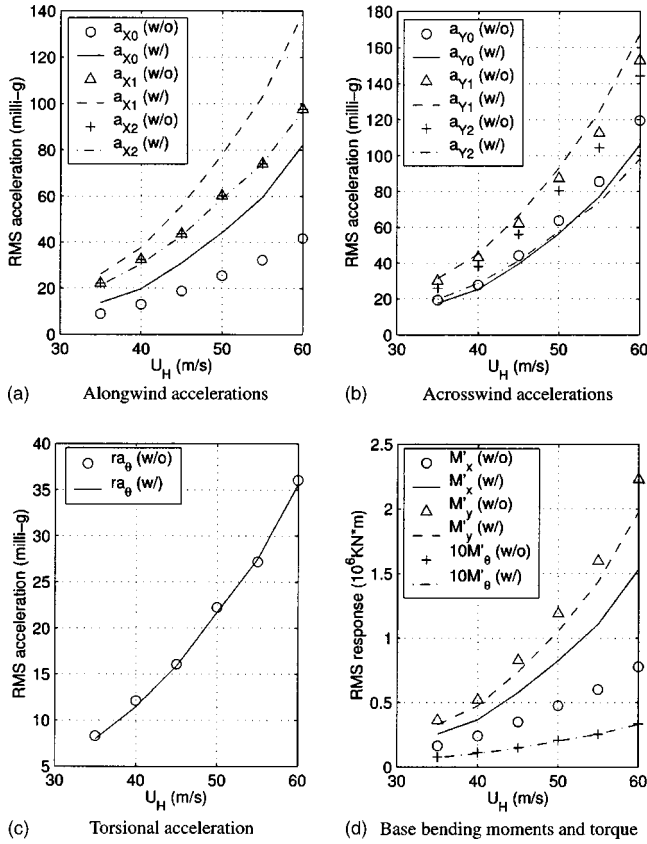


Fig. 3. Power spectral densities of measured base bending moments and torque



**Fig. 4.** Influence of eccentricity on the building response: (a) alongwind accelerations; (b) crosswind accelerations; (c) torsional acceleration; and (d) base bending moments and torque

frequencies are 0.1941, 0.2000, and 0.3090 Hz. The corresponding mode shapes are  $(\Theta_{jx} \Theta_{jy} \Theta_{j\theta}) = (\Psi_x \alpha_{jx} \Psi_y \alpha_{jy} \Psi_\theta \alpha_{j\theta})$  ( $j=1, 2, 3$ ) with  $(\alpha_{1x} \alpha_{1y} r_{\alpha_{1\theta}}) = (0.6929 - 0.6929 - 0.1997)$ ,  $(\alpha_{2x} \alpha_{2y} r_{\alpha_{2\theta}}) = (0.7071 \ 0.7071 \ 0.0000)$ , and  $(\alpha_{3x} \alpha_{3y} r_{\alpha_{3\theta}}) = (0.1412 - 0.1412 \ 0.9799)$ , respectively. The modal damping ratio for each mode is assumed to be 1%.

In this example, only the mean wind direction along axis  $x$ , i.e., normal to a face of the building, is considered. The mean wind speed at the building height varies between 35 to 60 m/s. The aeroelastic effects, if any, are neglected at this range of wind speeds. Fig. 3 shows the PSDs of the measured base bending moments,  $M_x(t)$  and  $M_y(t)$ , and torque,  $M_\theta(t)$ , using the HFFB technique in an urban boundary layer flow (Kijewski and Kareem 1998). The wind tunnel test data suggested almost negligible correlation between  $M_x(t)$  and  $M_y(t)$  and relatively high correlation between  $M_y(t)$  and  $M_\theta(t)$ . For the sake of illustration, the corre-

lation coefficient between  $M_y(t)$  and  $M_\theta(t)$  is taken as 0.7, i.e.,  $\sigma_{M_y\theta}^2 = 0.7\sigma_{M_y}\sigma_{M_\theta}$ , and their XPSD is given by  $S_{M_y\theta}(f) = 0.7\sqrt{S_{M_y}(f)S_{M_\theta}(f)}$ . The generalized forces associated with 3D mode shapes can be quantified through measured base bending moments and torque as

$$S_{Q_{jk}}(f) = \sum_{s=x,y,\theta} \sum_{l=x,y,\theta} \alpha_{js}\alpha_{kl}\eta_{js}(f)\eta_{kl}(f)S_{M_{sl}}(f) \quad (j,k=1,2,3) \quad (60)$$

where the mode shape corrections,  $\eta_{js}(f)$  ( $j=1, 2, 3; s=x, y, \theta$ ), are determined according to Eq. (49) for the case of high correlation ( $k_{zxf}H/U_H=0$ ) with  $\Theta_{j\theta}=1$  and  $\beta_s=1.2$  and  $\alpha_s$  assumed to be 0.3. This results in  $\eta_{jx}=\eta_{jy}=0.92/H$  and  $\eta_{j\theta}=0.52$ .

Both the background and resonant response components are calculated by modal analysis and the response is reported here as the total response. The response components considered are the alongwind and crosswind accelerations at the top of the building at the following locations: top center, Point 0,  $(x_0, y_0) = (0, 0)$ ; top corner, Point 1,  $(x_1, y_1) = (B/2, B/2)$ ; top corner, Point 2,  $(x_2, y_2) = (-B/2, -B/2)$ , which are later referred to as  $a_{x0}$  and  $a_{y0}$ ,  $a_{x1}$  and  $a_{y1}$ , and  $a_{x2}$  and  $a_{y2}$ , respectively. The torsional acceleration at the building top referred to as  $a_\theta$ , alongwind and crosswind base bending moment responses  $M'_x$  and  $M'_y$ , base shear forces  $F'_x$  and  $F'_y$ , and the base torque response  $M'_\theta$  are also calculated. All those response components are easily calculated in terms of the modal response. For example, the alongwind acceleration at Point 1 and the alongwind base bending moment are quantified as

$$\sigma_{a_{x1}}^2 = \sum_{j=1}^3 \sum_{k=1}^3 (2\pi f_j)^2 (2\pi f_k)^2 (\alpha_{jx} - \alpha_{j\theta}B/2)(\alpha_{kx} - \alpha_{k\theta}B/2)\sigma_{q_j}\sigma_{q_k}r_{jk} \quad (61)$$

$$\sigma_{M'_x}^2 = \frac{m^2 H^4}{3.2} \sum_{j=1}^3 \sum_{k=1}^3 (2\pi f_j)^2 (2\pi f_k)^2 \alpha_{jx}\alpha_{kx}\sigma_{q_j}\sigma_{q_k}r_{jk} \quad (62)$$

where  $\sigma_{q_j}$  = RMS value of the  $j$ th modal response; and  $r_{jk}$  = correlation coefficient between the  $j$ th and  $k$ th modes.

In Fig. 4, the predicted response of the building with and without eccentricity between the mass and resistance centers is shown, which highlights the influence of eccentricity on the building response. Selected results for the wind speed of 60 m/s are summarized in Tables 1 and 2. Without the eccentricity, the alongwind accelerations at two corners are equal, but greater than the response at the center due to the added contribution of the torsional response. The crosswind response is greater than the alongwind response. The torsional motion provides slightly different levels of contribution to the crosswind responses at the two corners, which is attributed to the correlation between the crosswind and

**Table 1.** Contributions of Modal Inertial Loads (Building without Eccentricity)

	Mode 1 $\sigma_{R_1} = \Gamma_1 \sigma_{q_1}$	Mode 2 $\sigma_{R_2} = \Gamma_2 \sigma_{q_2}$	Mode 3 $\sigma_{R_3} = \Gamma_3 \sigma_{q_3}$	Total (CQC) $\sigma_R$	Total (SRSS) $\sigma_R$
$M'_x$ ( $10^6$ KN m)	0.7790	0	0	0.7790	0.7790
$M'_y$ ( $10^6$ KN m)	0	2.2297	0	2.2297	2.2297
$F'_x$ ( $10^4$ KN)	0.6149	0	0	0.6149	0.6149
$F'_y$ ( $10^4$ KN)	0	1.7599	0	1.7599	1.7599
$M'_\theta$ ( $10^4$ KN m)	0	0	3.3593	3.3593	3.3593

$r_{1,2}=r_{2,1}=0$ ;  $r_{1,3}=r_{3,1}=0$ ;  $r_{2,3}=r_{3,2}=0.0609$

Note: CQC=Complete quadratic combination; SRSS=Square root of the sum of squares.

**Table 2.** Contributions of Modal Inertial Loads (Building with Eccentricity)

	Mode 1 $\sigma_{R_1} = \Gamma_1 \sigma_{q_1}$	Mode 2 $\sigma_{R_2} = \Gamma_2 \sigma_{q_2}$	Mode 3 $\sigma_{R_3} = \Gamma_3 \sigma_{q_3}$	Total (CQC) $\sigma_R$	Total (SRSS) $\sigma_R$
$M'_x$ ( $10^6$ KN m)	1.3206	1.1809	0.0751	1.5341	1.7732
$M'_y$ ( $10^6$ KN m)	-1.3206	1.1809	-0.0751	1.9778	1.7732
$F'_x$ ( $10^4$ KN)	1.0424	0.9321	0.0592	1.2108	1.3996
$F'_y$ ( $10^4$ KN)	-1.0424	0.9321	-0.0592	1.5611	1.3996
$M'_\theta$ ( $10^4$ KN m)	-1.9013	0	2.6010	3.3113	3.2219

$r_{1,2}=r_{2,1}=-0.2532$ ;  $r_{1,3}=r_{3,1}=-0.0591$ ;  $r_{2,3}=r_{3,2}=0.0603$

Note: CQC=Complete quadratic combination; SRSS=Square root of the sum of squares.

torsional loads. The presence of eccentricity significantly amplifies the alongwind responses at Points 0 and 1, while the alongwind response at Point 2 remains almost the same as for the building without eccentricity. The eccentricity results in a decrease in the acrosswind response at Point 0 while the acrosswind response at Point 1 increases. The acrosswind response at Point 2 is remarkably decreased. Similar observations regarding the displacements were made but are not presented here for brevity. Accordingly, the eccentricity results in apparent increase in the alongwind base bending moment and a slight decrease in the acrosswind base bending moment. The torsional acceleration and base torque, which are mainly contributed by the third mode characterized by the dominant torsional motion, remain almost the same as the building without eccentricity. However, the torsional displacement is significantly amplified which is primarily contributed by the first mode as the contribution from the third mode decreases (see Tables 1 and 2 for  $M'_\theta$ ).

A comparison between the base bending moments and torque with and without taking into account the correlation of modal responses, which correspond to the CQC and SRSS combination schemes, respectively, is presented in Fig. 5. At the wind speed of 60 m/s, the correlation coefficients for the building with eccentricity are  $r_{1,2}=r_{2,1}=-0.2532$ ,  $r_{1,3}=r_{3,1}=-0.0591$ ,  $r_{2,3}=r_{3,2}=0.0603$ , which are calculated based on Eq. (11) over the frequency range from 0 to  $+\infty$ . Eqs. (12), (52), and (59) result in almost the equal estimate of  $r_{1,2}$ , but may not provide accurate estimations of  $r_{1,3}$  and  $r_{2,3}$ , due to their well separated frequencies. Nevertheless, those values are very small and therefore may be simply assumed as zero. The correlation between the first and second modal response results in a slight decrease in the along-

wind response and an increase in acrosswind response, whereas the base torque, mainly contributed by the third mode, remains almost unchanged.

Fig. 6 shows the influence of cross-correlation of wind loads acting in different directions on the building response. In this example, only the cross-correlation between the acrosswind and torsion is considered. Results show that cross-correlation of wind loads does not introduce a significant influence on the response. This observation may not be necessarily true for other wind directions in which wind loads acting in different directions may become strongly correlated.

The background response components are shown in Fig. 7. The solid lines show the results based on the proposed scheme that are directly derived from the measured base forces without any correction procedure. It is noteworthy that the proposed scheme provides exact predictions of the base bending moments and torque. The dots show the results based on the modal analysis which entails calculation of the generalized forces involving modal shape correction procedure. It is clear that due to the introduction of mode shape corrections, which are less than unity in this example, the predicted values based on the generalized forces are less than the measured ones, particularly for the torsional response.

In Fig. 8, the ratio of the RMS background response to the total response is shown. The ratio decreases with an increase in the wind speed. It is also noted that the background response contributes more to the torsional response as compared to the alongwind and acrosswind response components. The preceding trend of reduction in the background response can be approximately identified by examining the PSDs of the measured base

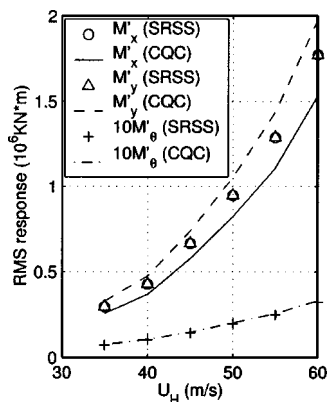


**Fig. 5.** Influence of correlation among modal responses

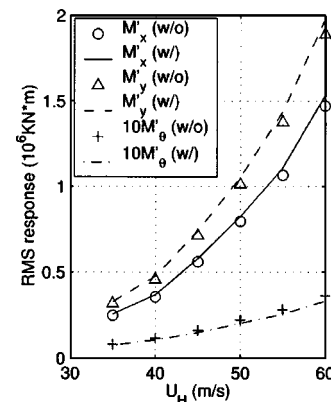


**Fig. 6.** Influence of cross correlation of wind loads acting in different directions

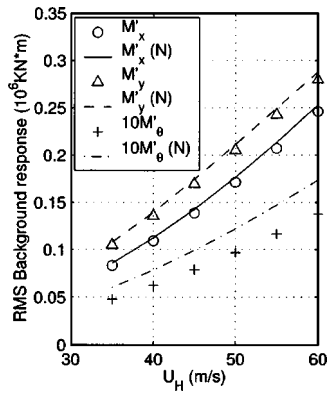


Fig. 7. Comparison of background response

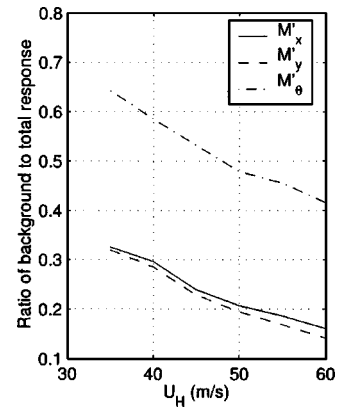


Fig. 8. Ratio of background to total response

forces, which represent the generalized forces. For example, the reduced frequencies for the fundamental modes in this example are 0.1719, 0.1771, and 0.2737 at wind speed of 35 m/s and 0.1000, 0.1030, and 0.1597 at 60 m/s. With the increase in wind speed, the reduced frequency decreases and the normalized amplitudes of the PSD at the modal frequencies increase concomitantly, which results in higher contributions to the resonant response as compared to the background response. It should be mentioned that these ratios will also depend on the modal damping of the building as well.

### Equivalent Static Wind Loads

The peak modal inertial loading for the three fundamental modes,  $F_{ejs}(z)$  ( $s=x, y, \theta; j=1, 2, 3$ ) with a peak factor of 3.5, which include both the background and resonant components, are shown in Fig. 9. The alongwind and acrosswind loads are expressed in terms of load per unit height, whereas the torque is given in terms of torque per unit height divided by the radius of gyration. These loads are the same as those obtained by distributing the base bending moments and torque over the building height in each fundamental mode. The ESWL for any peak response of interest can be expressed in terms of a linear combination of these load distributions.

The weighting factors of the peak modal inertial loads for selected response components are summarized in Table 3, which are calculated based on the proposed framework. For example, regarding the alongwind base bending moment, the weighting factor of the first modal inertial load is calculated as  $W_1 = [(1.3206 + 1.1809(-0.2532) + 0.0751(-0.0591))] / 1.5341 = 0.6630$  for the case with modal coupling, and  $W_1 = 1.3206 / 1.7732 = 0.7448$  for the case without modal coupling. The ESWL with modal coupling is then given by

$$F_{es}(z) = 0.6630F_{e1s}(z) + 0.5548F_{e2s}(z) + 0.0445F_{e3s}(z) \quad (63)$$

$(s = x, y, \theta)$

Using the methodology presented in this study, the ESWL for any peak response can be conveniently determined for immediate applications to building design.

### Concluding Remarks

The analysis of 3D coupled response and the quantification of ESWL for a given peak response of buildings with 3D coupled

mode shapes of vibration were presented. In this context, the spatiotemporally varying dynamic wind loads may be derived through multiple point synchronous scanning of pressures on the building model surface. Both the cross correlation of wind loads acting in different directions and intermodal coupling among modal response components were taken into consideration in the analysis of response and modeling of ESWL. The ESWL was expressed as a linear combination of the background and resonant loads characterized by fluctuating wind loads and inertial loads in fundamental modes of vibration. The background load, based on the gust loading envelope, offered a very convenient and physically meaningful description with an advantage over the LRC approach, which results in a unique spatial load distribution for each response component. The modeling of ESWL for spatiotemporally varying dynamic wind loads is not only very attractive for simplifying wind loads in building codes and standards, but also serves as a valuable framework for direct utilization of wind tunnel data for design application. The ESWL permits a relatively simple static analysis for response estimates.

The HFFB technique, primarily suitable for buildings with 1D uncoupled modes, was considered here for buildings with 3D coupled modes. The estimation of the generalized forces associated with 3D coupled modes with mode shape corrections were examined. It was noted that the mode shape corrections used for the case of uncoupled modes can be applied to coupled modes following the proposed methodology. A new scheme was presented for quantifying the background response by directly using the measured base forces without introducing any correction procedure. This scheme was predicated on the assumption that the background response of tall buildings is mainly contributed by their fundamental modes. Both the background and resonant ESWL distributions can be expressed in terms of modal inertial loads, which can be viewed as the base bending moments and torque in each mode distributed over the building height.

The predicted coupled response of an example tall building with eccentric structural system in terms of noncoincident centers of mass and resistance demonstrated the influence of eccentricity on building response to winds. The eccentricity resulted in an apparent increase in the alongwind base bending moment with a slight decrease in the acrosswind base bending moment. The base torque remained almost the same, which is primarily contributed by the fundamental mode dominated by the torsional motion. The example also showed that the cross correlation between the acrosswind and torsional wind loads and intermodal coupling of modal responses did not significantly influence the response, but these features may have marked influence on the response in

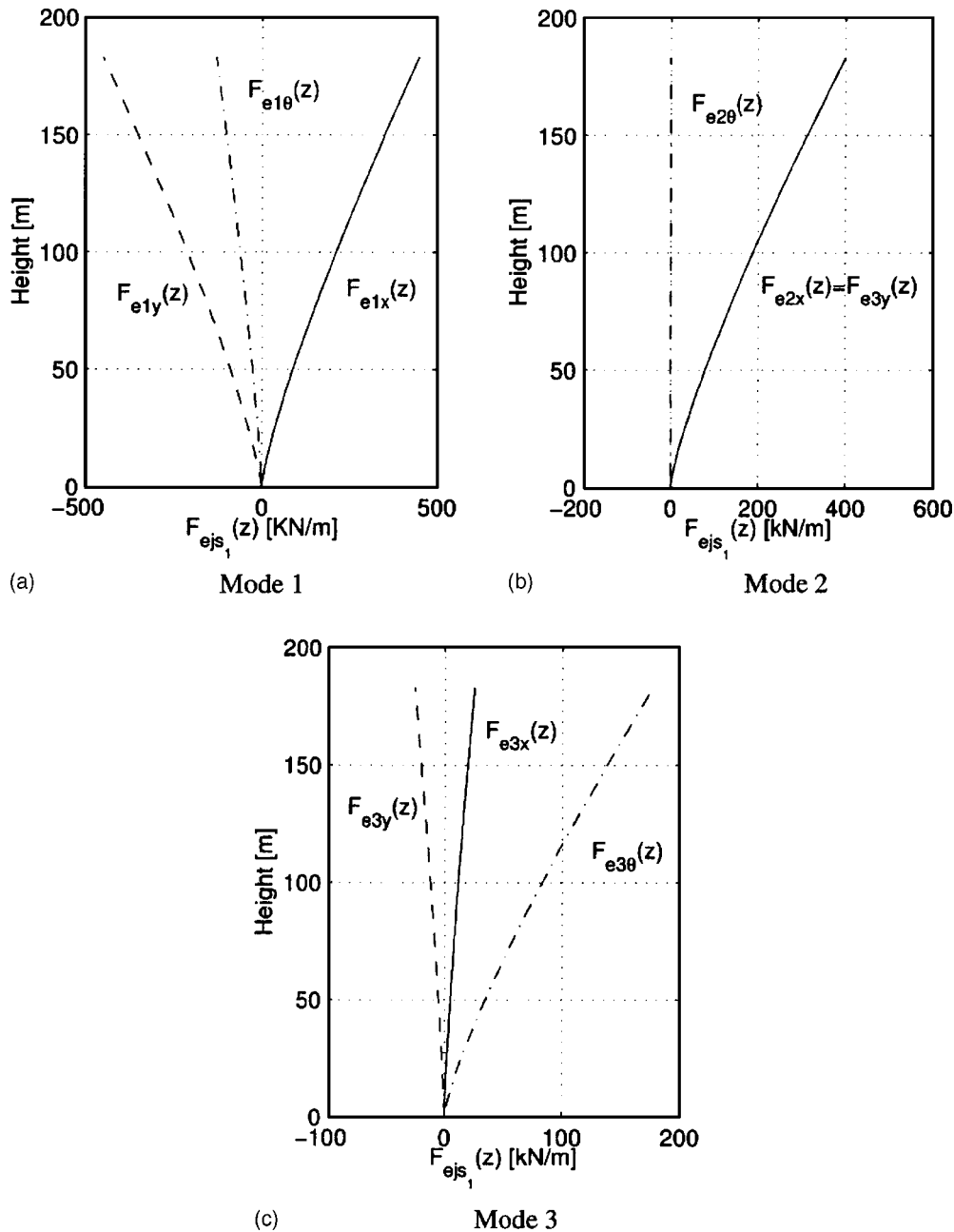


Fig. 9. Peak modal inertial load distributions: (a) Mode 1; (b) Mode 2; and (c) Mode 3

Table 3. Weighting Factors of Modal Inertial Loads

	With modal coupling (CQC)			Without modal coupling (SRSS)		
	$W_1$	$W_2$	$W_3$	$W_1$	$W_2$	$W_3$
$M'_x$	0.6630	0.5548	0.0445	0.7448	0.6660	0.0423
$M'_y$	-0.8167	0.7639	0.0375	-0.7448	0.6660	-0.0423
$F'_x$	0.6630	0.5548	0.0445	0.7448	0.6660	0.0423
$F'_y$	-0.8167	0.7639	0.0375	-0.7448	0.6660	-0.0423
$M'_θ$	-0.6206	0	0.8194	-0.5901	0	0.8073

Note: CQC=Complete quadratic combination; SRSS=Square root of the sum of the squares.

other wind directions or for different building dynamic characteristics. Different response components exhibited a distinct trend for a given eccentricity. The example also illustrated the procedure for evaluating the 3D building response and associated ESWL derived from the measured base forces. The proposed framework presented here has an immediate design application for buildings with 3D coupled modes based on either the synchronously scanned pressures on building surfaces or the HFFB measurements.

#### Acknowledgment

The support for this work was provided in part by NSF Grant No. CMS 00-85019. This support is gratefully acknowledged.

## Appendix. Equations of Motion for a Building with Eccentricity

It is assumed that the mass centers of all floors lie on one vertical axis so that the eccentricity between the centers of mass and resistance at each story level is the same and all floors have the same radius of gyration about the vertical axis through the mass center (Fig. 2). The origin of the coordinate system for building motions is defined at the mass center of the building. Only the coupling among the fundamental modes in the three primary directions are considered. The mode shapes of the uncoupled building system are denoted as  $\Psi_x(z)$ ,  $\Psi_y(z)$ , and  $\Psi_\theta(z)$ , for each fundamental mode. Expressing the coupled response of the building system in terms of the mode shapes of the uncoupled building system as  $X(z)=\Psi_x(z)\alpha_x$ ,  $Y(z)=\Psi_y(z)\alpha_y$  and  $\Theta(z)=\Psi_\theta(z)\alpha_\theta$ , the equations of motion of the building excluding the building damping can be expressed as (e.g., Kareem 1985)

$$\mathbf{M}_0\ddot{\mathbf{q}}_0 + \mathbf{K}_0\mathbf{q}_0 = \mathbf{Q}_0 \quad (64)$$

$$\mathbf{M}_0 = \begin{bmatrix} m_0 & 0 & 0 \\ 0 & m_0 & 0 \\ 0 & 0 & m_0 \end{bmatrix}; \quad \mathbf{K}_0 = \begin{bmatrix} K_x & 0 & -e_y/rK_x \\ 0 & K_y & e_x/rK_y \\ -e_y/rK_x & e_x/rK_y & K_\theta \end{bmatrix}; \quad (65)$$

$$\mathbf{q}_0 = (\alpha_x \quad \alpha_y \quad r\alpha_\theta)^T; \quad \mathbf{Q}_0 = (Q_x \quad Q_y \quad Q_\theta/r)^T \quad (66)$$

$$m_0 = \int_0^H \Psi_x^2(z)m(z)dz = \int_0^H \Psi_y^2(z)m(z)dz = \int_0^H \Psi_\theta^2(z)I(z)dz/r^2 \quad (67)$$

$$K_x = m_0\omega_x^2; \quad K_y = m_0\omega_y^2; \quad K_\theta = m_0(\omega_\theta^2 + e_x^2/r^2\omega_x^2 + e_y^2/r^2\omega_y^2) \quad (68)$$

$$Q_s = \int_0^H \Psi_s(z)P_s(z)dz \quad (s = x, y, \theta) \quad (69)$$

where  $m(z)$  and  $I(z)=r^2m(z)$ =mass and polar moment of inertia per unit height;  $\omega_s$  ( $s=x, y, \theta$ )=fundamental modal frequencies of the uncoupled building system;  $r$ =radius of gyration; and  $e_x$  and  $e_y$ =distances between the centers of mass and resistance in  $x$  and  $y$  directions.

By expressing  $\mathbf{q}_0$  as

$$\mathbf{q}_0 = \sum_{j=1,2,3} \mathbf{Y}_j q_j = \mathbf{Y}\mathbf{q} \quad (70)$$

$$\mathbf{q} = (q_1 \quad q_2 \quad q_3)^T; \quad \mathbf{Y} = [\mathbf{Y}_1 \quad \mathbf{Y}_2 \quad \mathbf{Y}_3];$$

$$\mathbf{Y}_j = (\alpha_{jx} \quad \alpha_{jy} \quad r\alpha_{j\theta})^T \quad (71)$$

where  $\mathbf{Y}_j$  satisfies the following eigenvalue problem

$$(-\omega_j^2\mathbf{M}_0 + \mathbf{K}_0)\mathbf{Y}_j = 0 \quad (72)$$

then the equations of building motion can be described in the following uncoupled equations including the modal damping term in terms of the generalized modal coordinates  $\mathbf{q}(t)$  as

$$\mathbf{M}\ddot{\mathbf{q}} + \mathbf{C}\dot{\mathbf{q}} + \mathbf{K}\mathbf{q} = \mathbf{Q} \quad (73)$$

$$\mathbf{M} = \text{diag}[m_j]; \quad \mathbf{C} = \text{diag}[2\xi_j m_j \omega_j]; \quad \mathbf{K} = \text{diag}[m_j \omega_j^2] \quad (74)$$

$$m_j = (\alpha_{jx}^2 + \alpha_{jy}^2 + (r\alpha_{j\theta})^2)m_0; \quad Q_j = \alpha_{jx}Q_x + \alpha_{jy}Q_y + (r\alpha_{j\theta})Q_\theta/r \quad (75)$$

where  $m_j$ ,  $\xi_j$ ,  $\omega_j$ , and  $Q_j$ = $j$ th generalized mass, damping ratio, frequency, and force ( $j=1,2,3$ );  $\alpha_{jx}$ ,  $\alpha_{jy}$ , and  $r\alpha_{j\theta}$ = $j$ th mode shape in terms of coordinates  $\alpha_x$ ,  $\alpha_y$  and  $r\alpha_\theta$ ; and accordingly  $(\Theta_{jx} \quad \Theta_{jy} \quad \Theta_{j\theta}) = (\Psi_x\alpha_{jx} \quad \Psi_y\alpha_{jy} \quad r\Psi_\theta\alpha_{j\theta})$ = $j$ th mode shape in the physical coordinates.

## References

- American Society of Civil Engineers (ASCE). (1999). *Wind tunnel studies of buildings and structures*, ASCE Manuals and reports on engineering practice No. 67, ASCE, New York.
- American Society of Civil Engineers (ASCE). (2002). "Minimum design loads for buildings and other structures." *ASCE 7-02*, ASCE, New York.
- Boggs, D. W., and Peterka, J. A. (1989). "Aerodynamic model tests of tall buildings." *J. Eng. Mech.*, 115(3), 618–635.
- Chen, X., and Kareem, A. (2001). "Equivalent static wind loads for buffeting response of bridges." *J. Struct. Eng.* 127(12), 1467–1475.
- Chen, X., and Kareem, A. (2004). "Equivalent static wind loads on tall buildings: New model." *J. Struct. Eng.* 130(10), 1425–1435.
- Davenport, A. G. (1967). "Gust loading factors." *J. Struct. Div. ASCE*, 93, 11–34.
- Davenport, A. G. (1985). "The representation of the dynamic effects of turbulent wind by equivalent static wind loads." *Proc. AISC/CISC Int. Symp. on Struct. Steel*, Chicago, 3-1–3-13.
- Davenport, A. G. (1995). "How can we simplify and generalize wind loads?" *J. Wind. Eng. Ind. Aerodyn.*, 54–55, 657–669.
- Der Kiureghian, A. (1980). "Structural response to stationary excitation." *J. Eng. Mech.* 106(6), 1195–1213.
- Flay, R. G. J., Yip, D. Y. N., and Vickery, B. J. (1999). "Wind induced dynamic response of tall buildings with coupled 3D modes of vibration." *Wind Engineering into 21st Century*, Larsen, Larose, and Livesey, eds., Balkema, Rotterdam, The Netherlands, *Proc., 10th Int. Conf. on Wind Eng.*, Copenhagen, Denmark, 645–652.
- Holmes, J. D. (1994). "Along-wind response of lattice towers. Part I: Derivation of expression for gust response factors." *Eng. Struct.* 16, 287–292.
- Holmes, J. D. (1996). "Along-wind of lattice towers. Part III: Effective load distribution." *Eng. Struct.* 18, 483–488.
- Holmes, J. D. (2002). "Effective static load distributions in wind engineering." *J. Wind. Eng. Ind. Aerodyn.* 90, 91–109.
- Holmes, J. D., Rofail, A., and Aurelius, L. (2003). "High-frequency base balance methodologies for tall buildings with torsional and coupled resonant modes." *Proc., 11th Int. Conf. on Wind Eng.*, 2381–2387.
- Irwin, P. A., and Xie, J. (1993). "Wind loading and serviceability of tall buildings in tropical cyclone regions." *Proc., 3rd Asia-Pacific Symp. on Wind Engineering*, Univ. of Hong Kong.
- Kareem, A. (1985). "Lateral-torsional motion of tall buildings." *J. Struct. Eng.*, 111(11), 2479–2496.
- Kareem, A., and Cermak, J. E. (1979). "Wind tunnel simulation of wind-structure interactions." *ISA Trans.*, 18(4), 23–41.
- Kareem, A., and Zhou, Y. (2003). "Gust loading factors—Past, present, and future." *J. Wind. Eng. Ind. Aerodyn.* 91(12–15), 1301–1328.
- Kasperski, M. (1992). "Extreme wind load distributions for linear and nonlinear design." *Eng. Struct.* 14, 27–34.
- Kijewski, T., and Kareem A. (1998). "Dynamic wind effects: A comparative study of provisions in codes and standards with wind tunnel data." *Wind Struct.*, 1(1), 77–109.
- Piccardo, G., and Solari, G. (2000). "Three-dimensional wind-excited response of slender structures: Closed-form solution." *J. Struct. Eng.* 126(8), 936–943.
- Reinhold, T. A., and Kareem, A. (1986). "Wind loads and building response predictions using force balance techniques." *Proc., 3rd Eng.*

- Mech. Conf.—Dynamic Response of Structures*, ASCE, New York, 390–397.
- Repetto, M. P., and Solari, G. (2004). “Equivalent static wind actions on structures.” *J. Wind. Eng. Ind. Aerodyn.*, 100(7), 1032–1040.
- Shimada, K., Tamura, Y., Fujii, K., and Wakahara, T. (1990). “Wind induced torsional motion of tall building.” *Proc., 11th National Symp. Wind Eng.*, 221–226 (in Japanese).
- Tallin, A., and Ellingwood, B. (1985). “Wind induced lateral-torsional buildings.” *J. Struct. Eng.*, 111(10), 2197–2213.
- Tschanz, T., and Davenport, A. G. (1983). “The base balance technique for the determination of dynamic wind loads.” *J. Wind. Eng. Ind. Aerodyn.* 13(1–3), 429–439.
- Vickery, P. J., Steckley, A. C., Isyumov, N., and Vickery, B. J. (1985). “The effect of mode shape on the wind induced response of tall buildings.” *Proc., 5th U.S. National Conf. Wind Eng.*, Texas Tech Univ., Lubbock, Tex., 1B-41–1B-48.
- Xie, J., Irwin, P. A., and Accardo, M. (1999). “Wind load combinations for structural design of tall buildings.” *Wind Engineering into 21st Century*, Larsen, Larose, and Livesey, eds., Balkema, Rotterdam, The Netherlands, *Proc. 10th Int. Conf. on Wind Eng.*, Copenhagen, Denmark, 163–168.
- Xie, J., Kumar, S., and Gamble, S. (2003). “Wind loading study for tall buildings with similar dynamic properties in orthogonal directions.” *Proc., 11th Int. Conf. Wind Eng.*, Lubbock, Tex., 2390–2396.
- Xu, Y. L., and Kwok, K. C. S. (1993). “Mode shape corrections for wind tunnel tests of tall buildings.” *Eng. Struct.*, 15, 618–635.
- Yip, D. Y. N., and Flay, R. G. J. (1995). “A new force balance data analysis method for wind response predictions of tall buildings.” *J. Wind. Eng. Ind. Aerodyn.*, 54/55, 457–471.
- Zhou, Y., and Kareem, A. (2001). “Gust loading factor: New model.” *J. Struct. Eng.* 127(2), 168–175.
- Zhou, Y., Kareem, A., and Gu, M. (2002). “Mode shape corrections for wind load effects.” *J. Eng. Mech.* 128(1), 15–23.
- Zhou, Y., and Kareem, A. (2003). “Aeroelastic balance.” *J. Eng. Mech.* 129(3), 283–292.